Xth International Conference on Thermoelectrics
Cardiff, Wales, UK, 10th - 12th Sept. 1991
Babrow Press, Cardiff, 1991, pp. 167-173.
D.M. Rowe, Ed.

Vining

INTRINSIC THERMOELECTRIC PROPERTIES OF SINGLE CRYSTAL Ru_2Si_3

Cronin B. Vining and C. E. Allevato

Jet Propulsion Laboratory, California Institute of Technology, Pasadena, California, USA

ABSTRACT

Single crystals of Ru_2Si_3 have been grown in boron nitride crucibles using a Bridgman-like method. Boron-rich precipitates about 1 μm wide by 20 μm long and occurring along regular crystallographic directions are observed representing about 1% by area of a typical cross-section. Hall effect, electrical resistivity and Seebeck coefficient measurements have been performed from 300 to 1300 K and thermal diffusivity has been determined from 600 to 1300 K, both parallel and perpendicular to the sample growth direction. Mobility values as high as 90 $cm^2/V\text{-}s$ have been observed at 700 K and thermal conductivity values as low as 24 mW/cm-K have been measured. Seebeck values vary from -200 μV/K to +400 μV/K. The longitudinal speed of sound has been determined as 6.32 km/s. A previously reported phase transformation at about 1250 K has been observed in single crystals. Simple analysis of the results and the potential of these materials for thermoelectric applications are discussed.

INTRODUCTION

While several transition-metal silicides have been previously studied, relatively little is known about the thermoelectric properties of many other transition-metal silicide semiconductors. Among these materials, ruthenium sesquisilicide Ru_2Si_3 was identified as particularly promising based on results on arc-melted samples (1) and more recently supported by results on polycrystalline Bridgman grown material (2). Analysis of the transport properties of these samples has lead to the speculation that figure of merit values for Ru_2Si_3 may be as much as 3 to 4 times higher than achieved in standard silicon-germanium alloys, assuming high quality, optimally doped samples can be prepared (1,2).

A distinguishing feature of the transition-metal silicides is the presence of d-bands, which are absent in semiconductors such as SiGe, PbTe and Bi_2Te_3. The higher effective mass (m_{eff}) values of the d-bands should contribute to higher Seebeck values. For some materials higher thermoelectric figure of merit values, roughly like $m^{3/2}\mu/\lambda_{lattice}$, can be expected, assuming the greater effective mass and lower thermal conductivity more than compensate for the (expected) decrease in the mobility.

Ru_2Si_3, closely related to the $TiSi_2$ structure type (3), is sometimes described as a Nowotny "chimney ladder" compound due to the common occurrence of long unit cells in one direction (4). Here, the metal atoms (e.g. Ru) occupy essentially a β-Sn crystal structure while the positions of the non-metal atoms (e.g. Si) vary somewhat from compound to compound. A large number of compounds have been identified with this basic crystal structure, including silicides, germanides, aluminides and gallides of Mn, Ru, Os, Rh and Ir, which suggests that many solid solutions may be possible in these systems.

A simple, but powerful, empirical rule has been identified for the prediction of semiconducting behavior in these materials: the so-called "magic rule" of 14 valence electrons per metal atom. Thus, the valencies (counting all outer shell electrons) of ruthenium (8) and silicon (4) gives (2x8 + 3x4)/2 = 14 valence electrons per ruthenium in Ru_2Si_3. Recent band-structure calculations (5) confirm that Ru_2Si_3 is a semiconductor with a band gap consistent with the "magic rule." Significantly, however, these calculations indicate that both the valence and conduction bands have significant d-band character, in sharp contrast to an earlier suggestion that the gap forms only after the entire d-band is filled (6).

The complex crystal structure, ability to form alloys and the heavy elements involved all suggest that low thermal conductivity values should be possible. The electronic structure indicates a band gap between states with large d-band character, which suggests that large Seebeck values should be possible. Thus, the lattice structure, electronic structure and potential for alloying all seem very favorable for thermoelectric applications.

These attributes, however, apply equally well to a number of the Nowotny compounds and the question of which particular compound to pursue experimentally may be decided by additional considerations. The only Nowotny compound previously studied for thermoelectric applications is $MnSi_{\sim 1.75}$ (actually a series of closely related compounds near this composition), which has been studied by several authors (7, 8, 9, 10, 11). These studies achieved ZT values as high as about 0.8, which is already rather encouraging (7, 11).

Ru_2Si_3 is a refractory, congruently melting (1973 K) compound with a phase diagram indicating no nearby, low-melting point eutectics (12). Being composed of only of low vapor pressure elements there is less chance that minor reactions or decompositions would result in volatile species. The closely related compound Os_2Si_3 may be even more attractive due to the higher mass of Os, but Ru_2Si_3 was selected for these initial experiments due to the greater cost of high purity Os compared to Ru.

The primary goal of the current study was to prepare high quality samples of undoped Ru_2Si_3 in order to reliably establish the intrinsic properties of the compound. A Bridgman-like preparation method was selected due to the relative simplicity of the method and the previously successful attempts to prepare the related compound $MnSi_{1.75}$ from the melt (7, 9, 11). A previous review of transition metal silicide preparation methods had suggested that no suitable container material was available for silicides'

with melting points above 1873 K (13). This difficulty was at least partially resolved in the current study by the use of a pyrolytic boron nitride crucible.

One question of particular interest is the reported polymorphism of Ru_2Si_3. Previous high temperature X-ray (14) and electrical resistivity (15) results suggest Ru_2Si_3 transforms from the orthorhombic Ru_2Ge_3 structure type at low temperatures via a diffusionless phase transformation to the tetragonal, Ru_2Sn_3 structure type above about 1273 K. The most recent phase diagram determination, however, observed only the orthorhombic Ru_2Ge_3 structure type (at room temperature, in quenched samples) and concluded the tetragonal phase, if it exists, must transform very rapidly to the orthorhombic phase upon cooling (12).

EXPERIMENTAL DETAILS

Samples were prepared from 99.997% ruthenium powder (Johnson Matthey, Puratronic grade) and 1-2 Ω-cm, n-type silicon (Wacker-Chemitronic). Stoichiometric quantities of the elemental powders were placed in a thin-walled, tapered pyrolytic boron nitride crucible (Union Carbide). The bottom of the crucible ends in a rounded tip with approximately a 2 mm radius of curvature. The crucible with charge was placed in a vertical, cylindrical, two-zone, graphite heating element furnace (Thermal Technologies) in an atmosphere of flowing helium. The temperature profile along the center axis of the furnace was determined in a separate experiment using an empty crucible. The temperature gradient was estimated to be 32 K/cm in the working region during the crystal growth.

After establishing the temperature gradient and raising the temperature to about 2038 K at the bottom of the crucible, the setpoint temperatures for both furnace heating elements were simultaneously lowered at the rate of 4 K/hr. Thus the estimated growth rate was about 1.2 mm/hr. After cooling below the melting point, the furnace power was cut off and the sample was quenched. Samples prepared previously using a slower cooling rate following the crystal growth procedure resulted in only polycrystalline ingots.

The resulting ingot appeared crack-free, had a metallic luster and weighed about 7 grams, within 0.1% of the weight of the original charge. The shape of the bottom of the ingot did not conform to the bottom of the crucible, indicating the presence of a gas trapped between the melt and the crucible during the crystal growth. Similar indications of trapped gas were observed in several other trial runs (2).

Sections of the ingot were cut and polished using standard metallographic techniques. The Hall effect, electrical resistivity, Seebeck coefficient and thermal diffusivity measurements were each performed on two different samples cut from the single crystal ingot. Both samples were irregularly shaped disks about 2 mm thick and lateral dimensions varying from 6 to 12 mm. One sample was cut with the face of the disk perpendicular to the [010] direction and the other sample was cut with the face of the disk perpendicular to the [001] direction, to within 9° in each case as determined by Laue back-reflection photographs. For the remainder of this paper, the designations (010) and [010] refer to measurements on the same sample, but (010) refers to a measurement in the plane of the disk such as electrical resistivity and Hall coefficient, while [010] refers to a measurement through the thickness of the disk, such as thermal diffusivity and Seebeck coefficient.

Hall effect and resistivity measurements were performed simultaneously between room temperature and 1300 K using a van der Pauws, four-point method (16). The precision of the resistivity and Hall coefficient are typically better than 1%. As the van der Pauw geometry assumes the material is isotropic, the accuracy of the resistivity and Hall data is in doubt, which will be discussed below. The Seebeck coefficient relative to niobium was determined on samples approximately 2 mm thick, from the slope of a ΔV versus ΔT plot (17). Seebeck values are estimated to have an accuracy of $\pm 10\ \mu VK$. Thermal diffusivity has been determined by a heat pulse method with an estimated error of ± 2-3% (18).

Heat capacity has been estimated using the high temperature Debye value of $C_p = 3\ k_B\ N \cong 3.03$ J/K-cm^3, where N is the total number of atoms/cm^3. The thermal conductivity has been calculated using the density, determined by immersion to be 6.90 ± 0.01 gm/cm^3 (within 1% of the theoretical density of 6.96 gm/cm^3), the measured thermal diffusivity and the calculated heat capacity. The longitudinal speed of sound has been measured as 6.32 km/s ±1 % by determining the time for a sound pulse to travel the length of the sample.

RESULTS

Laue back-reflection photographs performed on surfaces cut both perpendicular and parallel to the direction of growth indicated the ingot to be a single crystal with lattice parameters consistent with Poutcharovsky and Parté's values of a=11.057 Å, b=8.934 Å and c=5.533 Å (3). The growth direction was about 8.8° off from the [010] direction.

Figure 1 shows a back-scattered electron (BSE) image of Ru_2Si_3. The growth direction is toward the top of the micrograph which corresponds closely to the [010] direction. Linear features darker than the surrounding matrix are readily apparent in this figure. Most of the features present as either vertical or horizontal lines 100 to 300 μm long with a sub-micron width, corresponding to platelike inclusions parallel to the (010) and (100) planes.

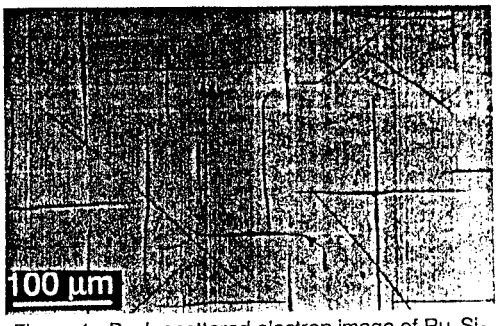

Figure 1: Back-scattered electron image of Ru_2Si_3 single crystal with boron-rich precipitates.

Many of these linear features exhibit a widening from sub-micron width to 1-2 μm wide regions along a portion (5 to 50 μm) of the inclusion. Figure 2 exhibits a detail of one of the wide zones in a BSE image and X-ray maps for the elements ruthenium, silicon and boron. In the BSE images the brighter

regions correspond to a higher average atomic number while in the X-ray maps the brighter regions indicate greater concentration of the element being examined. Thus the X-ray maps indicate the inclusions are deficient in ruthenium and silicon and rich in boron compared to the matrix material.

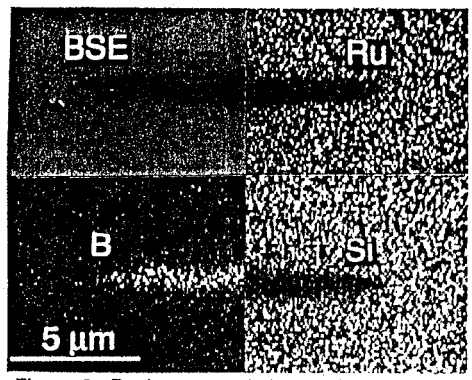

Figure 2: Back-scattered electron image and X-ray maps for ruthenium, silicon and boron for an inclusion in a Ru_2Si_3 single crystal.

The inclusion shown in Figure 2 is about 12 by 1.6 μm, which is slightly longer than the median length (~7 μm) and about the same width as the typical inclusion. These thicker features comprise about 1% of the area of the sample as determined using a digitized image analysis technique. These boron-rich inclusions are visible also in optical micrographs, although the contrast is not so strong in this case and many of the thinner extensions are not visible at all.

Figure 3 shows the similarity of the electrical resistivity for single crystal Ru_2Si_3 in the (001) and (010) planes. Over much of the temperature range the results of the measurements on the two samples agree to within 10 to 15%. Data points for the (001) sample are not shown for clarity.

At about 1240 K there is a sudden drop in the electrical resistivity of the (001) sample from about 0.012 to 0.006 Ω-cm, as shown in the inset to Figure 3. Upon cooling again through this temperature, the resistivity returns to the higher value with a small hysterysis. A much smaller step is also observed in the resistivity of the (010) sample.

Figure 4 shows the results of high temperature Hall effect measurements in the planes (010) and (001), plotted as the inverse of the Hall coefficient in units of cm^{-3}. The data for the (001) sample exhibit slightly greater random scatter due to the somewhat less favorable geometry of this sample.

The data are p-type over the entire temperature range and above 500 K the values for both samples agree to within a few percent. Between 600 K and 1240 K the apparent carrier concentration increases logarithmically with an activation energy of 0.54±0.02 eV, as indicated by the dashed line in Figure 4. Above 1240 K the apparent carrier concentration for the (010) sample increases suddenly from about 3.5 to about 11×10^{19} cm^{-3}, consistent with the sudden decrease in the resistivity at this temperature. The (001) sample also exhibits an increase in the apparent carrier concentration at this temperature, but the data are less reliable in this case due to noise.

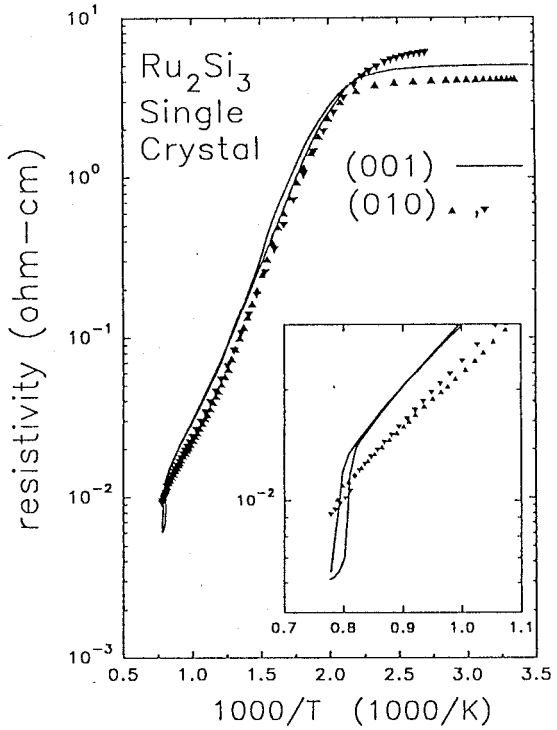

Figure 3: Electrical resistivity for single crystal Ru_2Si_3. The lines represents the (001) sample and the symbols represent the (010) sample. The inset shows an expanded view of the high temperature data.

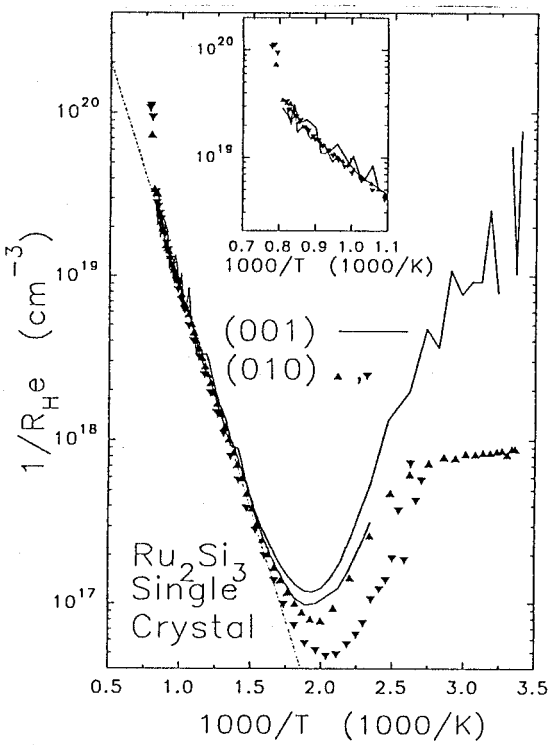

Figure 4: Inverse Hall coefficient in carrier concentration units for single crystal Ru_2Si_3. The solid lines represents the (001) sample and the symbols represent the (010) sample. The inset shows the high temperature data.

ure 5 shows the Hall mobility, defined as the ratio of the ll coefficient and the electrical resistivity, for single crystal $_2Si_3$. For both the (010) and (001) samples, the mobility 'eases with increasing temperature between 300 K and ɔut 700 K and then decreases with further increase in ıperature. Above 1240 K the (010) sample exhibits a ɨden decrease, while the mobility data on the (001) were reliable at these temperatures. Upon cooling, both nples exhibit peak mobility values about 30% higher than values on warming, and the peak values occur about 70 ɔwer in temperature. The mobility for the (010) sample ɔve 750 K is well described by

$$\mu_H = \frac{1.09 \times 10^5}{T} - 72.2 \ \text{cm}^2/\text{V-s}, \qquad (1)$$

indicated by the dashed line in Figure 5.

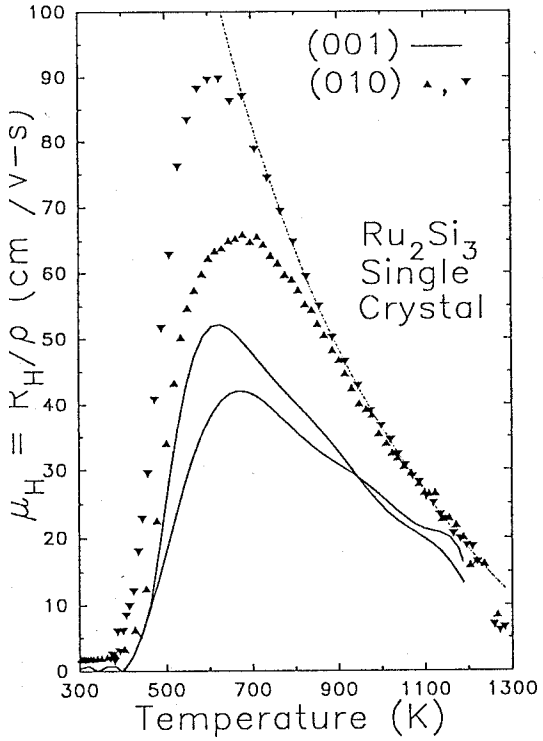

'igure 5: Hall mobility for single crystal Ru_2Si_3. The solid nes represents the (001) sample and the symbols epresent the (010) sample. The dashed line is given by ɨquation 1.

ıe intrinsic regime, a simple two band model with Hall ɨors equal to unity, yields

$$\mu_H = \mu_p - \mu_n \qquad (2)$$

the Hall mobility. The remarkably simple behavior of the ɜsured Hall mobility given in equation 1 suggests the ıtification of the first term as the hole mobility and the ɔnd term as the electron mobility. This identification will discussed below.

ure 6 shows the Seebeck coefficient for the two samples 0] and [001] of single crystal Ru_2Si_3. The Seebeck is ɜative at room temperature, rises sharply with increasing ıperature to a maximum of 400 to 450 μV/K at about 700 hen falls approximately linearly with increasing ıperature until around 1100 to 1200 K. At this ıperature, the Seebeck coefficient suddenly drops to a negative value. The temperature at which this sudden change in Seebeck occurs is about the same temperature at which the resistivity and Hall coefficient exhibit sudden changes.

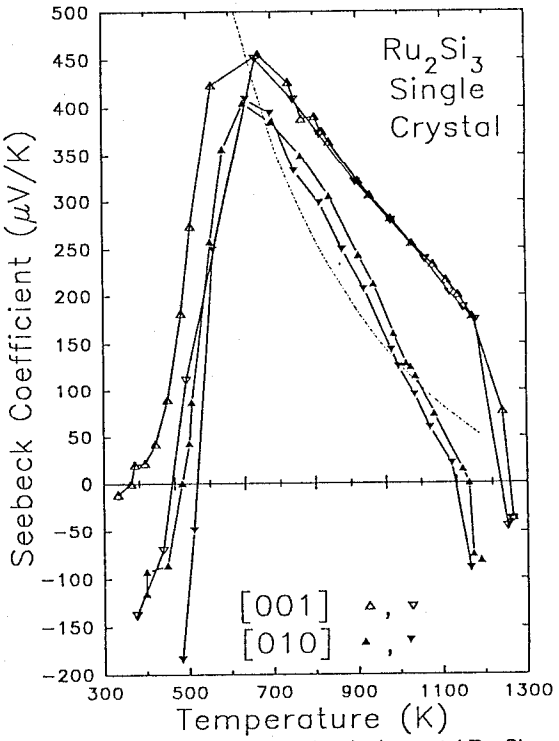

Figure 6: Seebeck coefficient for single crystal Ru_2Si_3. The solid lines are guides for the eye. The dashed line was calculated using equation 3.

The Seebeck coefficient for the [001] sample is generally higher than for the [010] sample and both samples exhibit more negative Seebeck coefficients at low temperatures after heating than they had before heating.

In a simple two band model, assuming acoustic scattering of carriers, the Seebeck coefficient in the extrinsic region is given by

$$S = \frac{k}{e}\left(2 + \frac{E_g}{2kT}\right)\frac{\mu_p - \mu_n}{\mu_p + \mu_n} + \frac{k}{e}\frac{3}{4}\ln\left(\frac{m_p}{m_n}\right) \qquad (3).$$

Taking

$$E_g = 2 \times 0.54 = 1.08 \text{ eV} \qquad (4a),$$

$$\mu_p = 1.09 \times 10^5/T \ \text{cm}^2/\text{V-s} \qquad (4b),$$

$$\mu_n = 72.2 \ \text{cm}^2/\text{V-s} \qquad (4c),$$

and neglecting the temperature independent ratio of the effective masses in equation 3a yields an estimate for the Seebeck coefficient given by the dashed line in Figure 6. This estimate is the correct order of magnitude and has approximately the same temperature dependence as the measured Seebeck coefficient, at least between 700 K and 1200 K.

Figure 7 shows the thermal conductivity of single crystal Ru_2Si_3 in the [001] and [010] directions. Also shown for comparison are previous results for polycrystalline Ru_2Si_3 prepared by arc-melting (1) and by the Bridgman method (2). The thermal conductivity typical of heavily-doped $Si_{0.8}Ge_{0.2}$

is also shown. The thermal conductivity of single crystal Ru_2Si_3 decreases rapidly with increasing temperature between 600 K and 950 K and then increases with increasing temperature. The thermal conductivity results in the [010] direction are generally higher than in the [001] direction, with a maximum difference of about 9% occurring around 950 K.

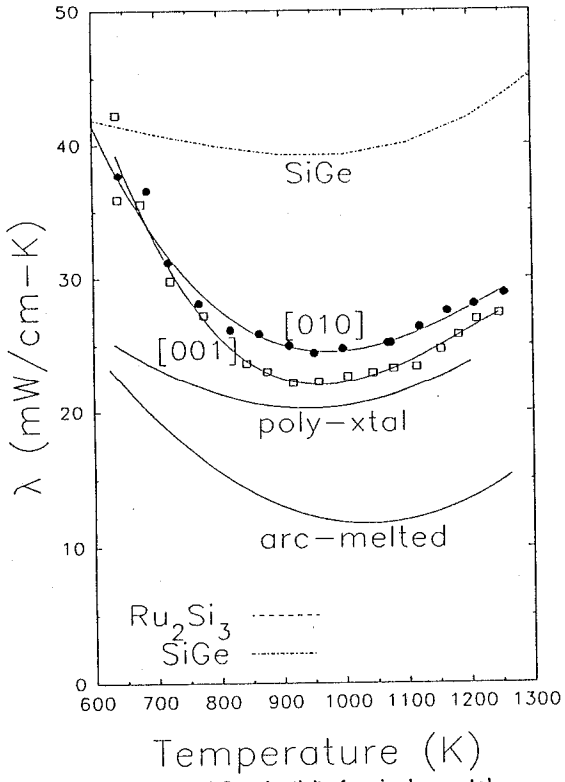

Figure 7: Thermal Conductivity for single crystal Ru_2Si_3 compared to heavily doped $Si_{0.8}Ge_{0.2}$ and two polycrystalline samples of Ru_2Si_3.

The electronic contribution to the thermal conductivity can also be estimated using the same assumptions described above for estimating the Seebeck coefficient. Thus

$$\lambda_{el} = \left[\frac{k}{e}\right]^2 \sigma T \left[2 + \frac{\mu_p \mu_n}{(\mu_p + \mu_n)^2}\left[4 + \frac{E_g}{kT}\right]^2\right] \qquad (5),$$

where the first term in the square brackets represents the usual non-degenerate Lorenz number and the second term represents the ambipolar contribution. Using the measured electrical resistivity and equations 4a-c to estimate the other parameters, yields the electronic contributions to the thermal conductivities for samples [010] and [001] shown in Figure 8. The calculated values of the lattice thermal conductivities are similar for the two samples, except at the highest temperatures where this calculation has the greatest uncertainties due to the strong temperature dependence and large size of the electronic component. The similarity of the lattice thermal conductivities for the two samples suggests the anisotropy is small.

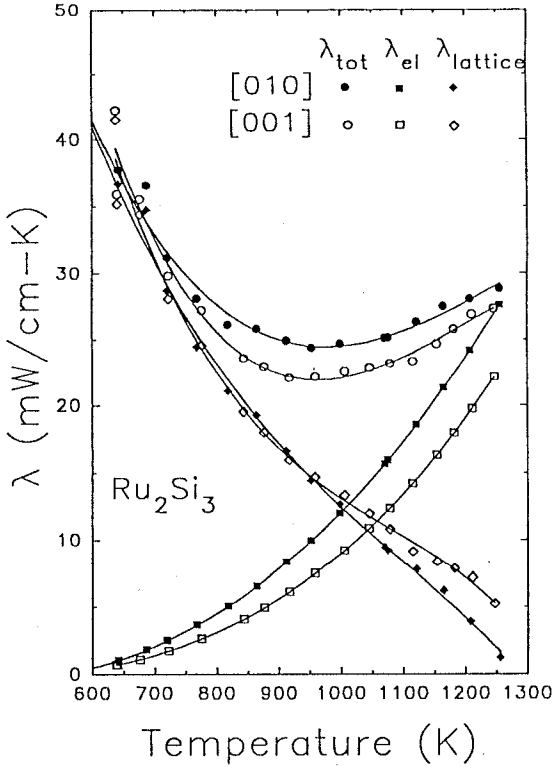

Figure 8: Electronic and lattice components of the thermal conductivity of Ru_2Si_3 for the [010] and [001] samples. The electronic component has been calculated using equations 4a-c and 5.

DISCUSSION

Both samples exhibit a sharp change in all three measured electronic transport properties at about 1240 K (perhaps slightly lower in the Seebeck coefficient). The magnitude of the change is relatively larger for the (001) sample. This would appear to represent a phase transformation, probably from the low temperature orthorhombic to the high temperature tetragonal structure discussed previously (14, 15) for arc-melted and annealed sample. Those results, however, describe a phase change which occurs gradually over a wide temperature, while in this study the phase change appears to be quite sharp. Presumably the difference in behavior is due to the single crystal nature of the current samples.

Interestingly, previous electrical measurements on polycrystalline samples prepared in this laboratory by arc-melting (1) and by directional crystallization (2) did not indicate a phase change, although the transition temperature could have been above the 1300 K limit of those measurements. Also related may be the observation that this single crystal was produced by removing the furnace power after the sample growth. Slower and more controlled post-growth cooling rates have produced only polycrystalline samples to date, perhaps due to this phase change.

Between about 700 K and 1240 K, Ru_2Si_3 appears to be a fairly ordinary semiconductor, resonably well described by a simple two-band model. The identification of the hole and electron mobilities as the temperature dependent and

temperature independent terms of equation 1 is not the only possibility, but this interpretation does predict the correct order of magnitude and qualitative temperature dependences for both the Seebeck coefficient and electronic component of the thermal conductivity, as shown in Figures 6 and 8. In any case, these estimates may be considered lower bounds for the mobilities.

The electrical and thermal conductivities for the two samples differ only slightly, except above 1240 K where the electrical resistivity of the (001) sample undergoes a much larger change than the (010) sample. The differences between the two samples in the intrinsic region would appear to be largely due to a difference in the mobilities.

The difference in the mobilities also qualitatively explains the relatively large difference in the intrinsic Seebeck coefficients in the two samples, which grows to over 150 μV/K just below the transition temperature, around 1200 K. From equation 3, the Seebeck coefficient (in the extrinsic regime) is expected to cross zero at about the same temperature as the Hall mobility, as given by equation 1. Figure 5 indicates the Hall mobility of the (001) sample should extrapolate to zero at a temperature well above the temperature at which the mobility of the (010) sample extrapolates to zero. A qualitatively similar effect is observed in the Seebeck coefficients for these two samples.

Since the Hall mobilities were determined in the plane of the sample disks, while the Seebeck coefficients were determined perpendicularly to the disks it is not clear precisely how to proceed with the analysis of these results. Also, as the dashed line in Figure 6 indicate, this simple model is only qualitatively reliable in any case. Moreover, it is not entirely clear whether these differences represent true anisotropy or merely some sort of inhomogeneity in the original single crystal ingot.

In most respects the Seebeck and Hall coefficient are in qualitative agreement with the interpretation of a donor-doped semiconductor which becomes intrinsically p-type as the temperature increases due to a larger intrinsic hole mobility compared to the electron mobility. Except in this case, unlike previous Hall measurements on polycrystalline samples (1 and 2), the Hall coefficient does not cross zero in the extrinsic region, but remains distinctly positive over the entire temperature range.

This, coupled with the apparent anisotropy in the high temperature Seebeck data, have prevented a reliable estimate of the hole and electron effective masses since no unambiguous interpretation of these results is yet available. Conceivably the unusual boron-precipitate microstructure plays some role.

In order to estimate of the potential of Ru_2Si_3 for thermoelectric applications, the properties of intrinsic Ru_2Si_3, reported here, are compared to the properties of an intrinsic "SiGe", with every effort to make conservative estimates. These estimates, appropriate for 1200 K, are summarized in Table 1. For the lattice thermal conductivity of "SiGe" a value of 27 mW/cm-K was used. This value, appropriate for 80% Si-20%Ge doped (hypothetically) to over $n=10^{21}$ cm^{-3}, was calculated using a model described in (19), and should be a fairly reliable lower limit.

For the intrinsic electron mobility, the acoustic-limited mobility of Si estimated using the parameters and methods described in (20) has been used. For the intrinsic hole mobility of "SiGe," the value 274 cm^2/V-s at 400 K estimated by Li (21), was scaled this using a $T^{-3/2}$ scaling law. In fact, the hole mobility of Si drops at a much faster rate. We take a hole effective mass of 1 (Li calculates 0.85 at 400 K) and an electron effective mass of 1.4 as estimated in (19).

TABLE 1 - Comparison of the intrinsic thermoelectric parameters of Ru_2Si_3 and SiGe at 1200 K.

type		m_{eff}	μ	$\lambda_{lattice}$	$m_{eff}^{3/2}\,\mu/\lambda_{lattice}$
p	Ru_2Si_3	4	91	10	72
p	Ru_2Si_3	1	91	10	9
p	SiGe	1	53	27	2
n	Ru_2Si_3	4	72	10	57
n	Ru_2Si_3	1	72	10	7
n	SiGe	1.4	188	27	12

Due to the uncertainty in the effective masses for Ru_2Si_3, two possibilities are examined. First, the smallest effective mass values estimated from two previous studies on Ru_2Si_3 are considered, which yielded values of about $m_{eff}=4$ for both electrons and holes. Second, we use effective mass values of unity for both electrons and holes, which considering the expected d-band nature of the band structure and effective masses observed in other transition-metal silicides $m_{eff}=1$ should be quite conservative indeed.

For "SiGe" we have used a lattice thermal conductivity value appropriate to a heavily doped alloy, while the value of 10 mW/cm-K for Ru_2Si_3 does not include these effects. The advantages of doping and alloying appear to be at least as promising for further lowering of the lattice thermal conductivity of Ru_2Si_3, since the single crystals studied here exhibit a temperature dependence close to the ideal 1/T behavior.

CONCLUSIONS

In the simplest models, the parameter $m_{eff}^{3/2}\,\mu/\lambda_{lattice}$ determines the thermoelectric figure of merit and a higher value predicts a higher figure of merit. From Table 1 it is clear that Ru_2Si_3 is quite promising indeed, particularly for p-type materials. Although the n-type materials should be useful also, and may be nearly as good as the p-type.

The usual cautions must be emphasized here with regard to these estimates. High figure of merit values have not yet been achieved in Ru_2Si_3. The promise indicated here can be realized only if: 1) high, extrinsic carrier concentrations can be achieved, 2) the mobilities decrease not too fast with increasing doping level, and 3) the observed phase transformation is not too serious. These formidable problems will be addressed in future studies.

ACKNOWLEDGEMENTS

The work described in this paper was carried out at the Jet Propulsion Laboratory, California Institute of Technology, under contract with the National Aeronautics and Space

Administration. The authors would like to thank P. Carpenter and R. Ruiz for their SEM work, L. Lowry for the X-ray analysis, and J. McCormack and A. Zoltan for assistance with the thermoelectric measurements. The authors would also like to thank Drs. A. Borshchevsky, J-P. Fleurial, M. Ryan, G. Slack and T. Ohta for helpful discussions.

REFERENCES

1. Vining, C.B., 1991, Proc. IX International Conference on Thermoelectrics (USA), Pasadena, CA, edited by C.B. Vining, (Jet Propulsion Laboratory Document D-7749), 249-259.
2. Ohta, T., Vining, C.B., and Allevato, C.E., 1991, Proc. 26th Intersociety Energy Conversion Engineering Conference, Boston, MA, in press.
3. Poutcharovsky, D.J., and Parthé, E., 1974, Acta Cryst., B30, 2692-2696.
4. Nowotny, H., 1970, "Crystal chemistry of transition element defect silicides and related compounds," in The Chemistry of Extended Defects in Non-Metallic Solids, edited by L. Eyring and M. O'Keeffe, 223-237.
5. Pecheur, P. and Toussaint, G., 1991, in Modern Perspectives in Thermoelectrics and Related Materials, (Materials Research Society Symposium Proceedings 234) edited by D. Allred, C. Vining and G. Slack, in press.
6. Jeitschko, W. and Parthé, E., 1967, Acta Cryst., 22, 417-430.
7. Bienert, W.B. and Skrabek, E.A., 1966, Proc. IEEE/AIAA Thermoelectrics Specialists Conference, 10.1-10.11.
8. Ivanova, L.D., Abrikosov, N. Kh., Elagina, E.,I., and Khvostikova, V.D., 1969, Inorganic Materials, 5(11), 1645-1648.
9. Levinson, L.M., 1973, J. Solid State Chem., 6, 126-135.
10. Zwilling, G. and Nowotny, H. , 1974, Monatshefte für Chemie, 105, 666-670 (in German).
11. Vednernikov, M.V., Engalychev, A.E., Zaitsev, V.K., Ordin, S.V., and Fedorov, M.I., 1988, Proc. 7th International Conference on Thermoelectrics, Arlington, TX, 150-155.
12. Weitzer, F., Rogl, P. and Schuster, J.C., 1988, Z. für Metallkunde, 79(3), 154-156.
13. Mason, K. N., 1979, Prog. Crystal Growth Charct., 2, 269-307.
14. Poutcharovsky, D.J., Yvon, K. and Parthé, E., 1975, J. Less Common Metals, 40, 139-144.
15. Susz, C.P., Muller, J., Yvon, K., and Parthé, E., 1980, J. Less Common Metals, 71, P1-P8.
16. McCormak, J., and Fleurial, J.-P., 1991, in Modern Perspectives in Thermoelectrics and Related Materials, (Materials Research Society Symposium Proceedings 234) edited by D. Allred, C. Vining and G. Slack, in press.
17. Wood, C., Zoltan, D., and Stapfer, G., 1985, Rev. Sci. Instrum., 56, 719.
18. Vandersande, J.W., Zoltan, A., and Wood, C., 1989, International J. Thermophysics, 10, 251-258.
19. Vining, C. B. , 1991, J. Applied Physics, 69, 331-341.
20. Li, S.S. and Thurber, W.R., 1977, Solid-State Electronics, 20, 609.
21. Li., S.S., 1978, Solid-State Electronics, 21, 1109-1117.